RSC Advances

Cite this: *RSC Advances*, 2012, **2**, 9786–9790

www.rsc.org/advances

COMMUNICATION

Hierarchical NiO hollow microspheres: electrochemical and magnetic properties†

Hyun Gil Cha,‡[a] Jong Hwa Sohn,‡[a] Youngjin Park,[a] Kyu Joon Lee,[b] Myung Hwa Jung,[b] Jae-won Lee,[c] Woonsup Shin,[a] Myung Jong Kang,[a] Do Yoon Kim[a] and Young Soo Kang*[a]

Received 26th January 2012, Accepted 13th August 2012
DOI: 10.1039/c2ra20910a

The interesting electrochemical performances and magnetic properties of hierarchical NiO hollow microspheres were investigated. A rational formation mechanism of NiO hollow spheres from $Ni(OH)_2$ was proposed on the basis of agglomerated-mediated growth.

Over the past few years, nanoscale materials with special morphologies have attracted intensive interest, because the intrinsic properties of nanoscale materials are mainly determined by their composition, crystallinity, size, and morphology. Nanoparticles often demonstrate novel properties different from those of bulk materials, and they can be used as fundamental building blocks for nanoscale science and technology.[1]

Recently, several reports have shown that metal nanoparticles can be assembled to form hierarchical porous spheres over multiple length scales with enhanced properties compared with both discrete nanoparticles and bulk powders. Moreover, the hollow spheres consisting of nanostructured materials also exhibit distinctive properties different from those of the nanoparticles.[2]

Rock salt structured (M = Fe, Co, Ni, Cu, …) transition metal oxides react reversibly with lithium in a lithium cell below 1.5 V.[3] It has been reported that the M–O type oxides demonstrate large capacity (700 mAh g^{-1}), long cycle life, and high recharging rates. These brilliant properties make them promising candidates for use as anode materials for Li-ion batteries.[4] Among them, nickel oxide is an interesting material due to its applications in diverse fields, including catalysis,[5] electrochromic films,[6] fuel cell electrodes,[7] gas sensors,[8] smart window,[9] and lithium-ion batteries.[10]

Also, NiO is an important transition metal oxide which has been preferred due to its interesting magnetic properties. Bulk crystals of NiO possess a rhombohedral structure and exhibit antiferromagnetic behavior below 523 K (T_N), whereas it has a cubic (NaCl-type) structure and it is paramagnetic above that temperature. It has been previously suggested that fine particles of NiO should exhibit weak ferromagnetism or superparamagnetism.[11]

Morphology-controlled synthesis and large-scale self-assembly of nanoscale building blocks into complex structures are of significant interest in materials and device fabrications.[12] For the construction of hollow spheres with hierarchical wall structures, surfactants or tri-block copolymers are usually required as structure-directing reagents.[13] Walsh and Mann reported the fabrication of hollow shells of skeletal-structured calcium carbonate from oil–water–surfactant microemulsions using polystyrene beads as the substrate.[14] Therefore, the creation of the hierarchical porous hollow structure with several kinds of combined structures is of great significance. Herein, we demonstrated that hierarchical nickel oxide hollow microstructures with porous nanosheets as the *in situ* formed building units were successfully fabricated by hydrothermal process and calcination in air.

As illustrated in Fig. 1, we designed a two-step procedure to produce the hierarchical NiO hollow spheres with meso- and macroporosity. On the basis of the all results in this study, we propose a possible agglomerated-mediated growth mechanism of hollow spheres with two-dimensional nanosheets. It is similar to the mesocrystal formation mechanism.[15]

$$Ni^{2+} + 6NH_3 \rightarrow [Ni(NH_3)_6]^{2+} \quad (1)$$

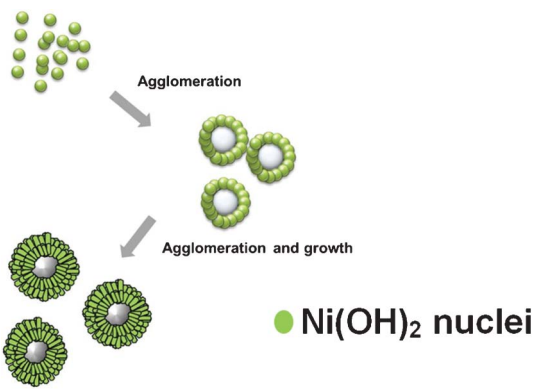

Fig. 1 Schematic illustration of the formation of hierarchical $Ni(OH)_2$ hollow spheres.

[a]*Korea Center for Artificial Photosynthesis, Department of Chemistry, Sogang University, Seoul 121-742, Republic of Korea. E-mail: yskang@sogang.ac.kr*
[b]*Department of Physics, Sogang University, Seoul 121-742, Republic of Korea*
[c]*Department of Energy Engineering, Dankook University, Cheonan 330-714, Republic of Korea*
† Electronic Supplementary Information (ESI) available. See DOI: 10.1039/c2ra20910a
‡ These authors contributed equally to the research work.

$$NH_3 + H_2O \rightarrow NH^{4+} + OH^- \quad (2)$$

$$Ni^{2+} + 2OH^- \rightarrow Ni(OH)_2 \quad (3)$$

In the beginning, the Ni^{2+} under an ammonia aqueous solution forms a relatively stable complex, $[Ni(NH_3)_6]^{2+}$. Afterwards, the complex is decomposed and releases NH_3 to provide OH^- ions for the formation of $Ni(OH)_2$ by hydrothermal treatment.

The formation of $[Ni(NH_3)_6]^{2+}$ complex would decrease the concentration of free Ni^{2+} ions in the solution, which resulted in a relatively low reaction rate of Ni^{2+} ions. A slow reaction rate caused the separation of the nucleation and growth steps, which is crucial for high-quality crystal synthesis. As a result, sheet-like high crystalline $Ni(OH)_2$ was formed, which may be related to the nature of the initial crystal growth. Then hierarchical $Ni(OH)_2$ hollow spheres were made by self-assembly and agglomerated-mediated growth. The crystal structure and chemical composition of the materials are analysed by XRD pattern and EDX spectrum, with the result shown in Fig. 2A and D. All the identified diffraction peak can be unambiguously assigned to the hexagonal $Ni(OH)_2$ (JCPDS card no. 14-0117).[16] No diffraction peak from impurities was found in the samples. In EDX spectrum, the element ratio of Ni and O is about 1 : 2.6.

The morphology of the sample is further examined by SEM in Fig. 2B. It shows that the product is composed of spherical particles with a diameter of ~6.3 μm. It can also be clearly identified that the spheres are composed of densely packed sheet-like subunits with relatively the same size and thickness. The hollow interior of these spheres is confirmed by TEM analysis in Fig. 2C, where they are shown to have a large void space and a well-defined shell. With a closer examination, the nanosheets subunits can be easily observed. Such an interesting structure causes the sample to have a high surface area of 13.9 $m^2\ g^{-1}$, with a relatively wide pore size distribution obtained by the nitrogen adsorption-desorption isotherm and Barret–Joyner–Halenda (BJH) methods. The SAED pattern further verifies that the hollow sphere is consistent with the agglomerated nanosheet due to a polytype ring pattern. It matches with the reflections corresponding to XRD results.

The magnetic properties of $Ni(OH)_2$ hollow spheres were investigated in Fig. 3. It has been reported that the bulk $Ni(OH)_2$ shows an antiferromagnetic (AFM) transition at the Neel temperature (T_N = 30 K). Takada *et al.* reported that bulk $Ni(OH)_2$ was an antiferromagnet exhibiting a metamagnetic property and a field-induced transition to place when the applied field was larger than the critical field.[17] The peak at around 19 K would be the freezing temperature of the AFM phase. The decrease in the ordered temperature of $Ni(OH)_2$ compared with 30 K is due to the decrease in grain size of $Ni(OH)_2$. The grain size of the nanosheet is about several nanometers, which is agglomerated on the surface of microsphere. The decrease of FC magnetization with decreasing temperature below 19 K indicated that this is a transition from paramagnetic (PM) to AFM. Moreover, the deviation between zero field cooling (ZFC) and field cooling (FC) is associated with the superparamagnetic behavior with spontaneous magnetization. It was confirmed as a cusp in the region at 25 K. As shown in Fig. 3B and C, we observed the hysteresis with the coercive field (H_c) at 5 K and no hysteresis at 300 K above T_b. The hysteresis loop at 300 K shows a linear curve above the Neel temperature due to the antiferromagnetic material. We also observed a clear metamagnetic transition at 5 K that occurs up to an applied field of 50 kOe. This originated from size and the interfacial effects, which would greatly affect the interaction between spin moments. Metamagnetic transition may occur when H exceeds the value $H_c = (2H_eH_a)^{1/2}$, at $T = 0$, where H_e

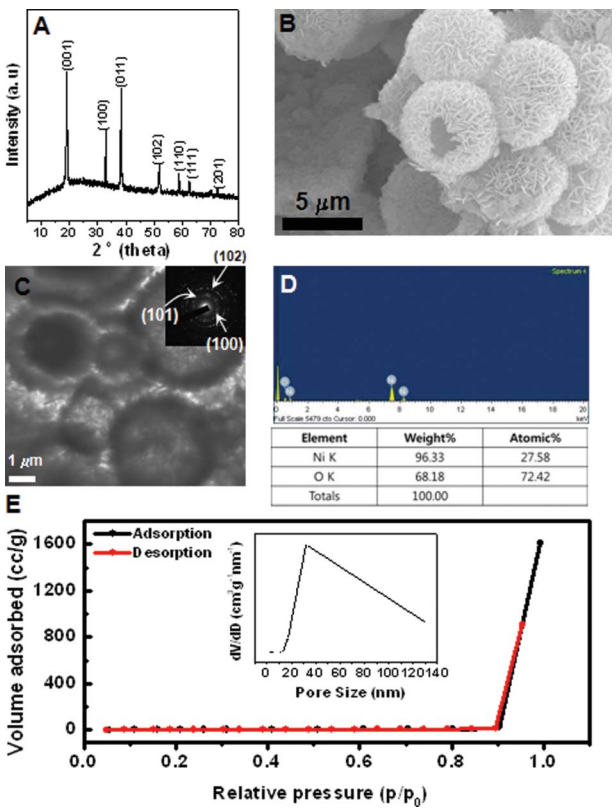

Fig. 2 (A) XRD, (B) SEM, (C) TEM, (D) EDX spectrum, and (E) N_2 adsorption-desorption isotherm of prepared hierarchical $Ni(OH)_2$ hollow spheres. Inset is pore-size distribution curve obtained from the desorption data. Inset are SAED patterns and pore-size distribution curve obtained from the desorption data.

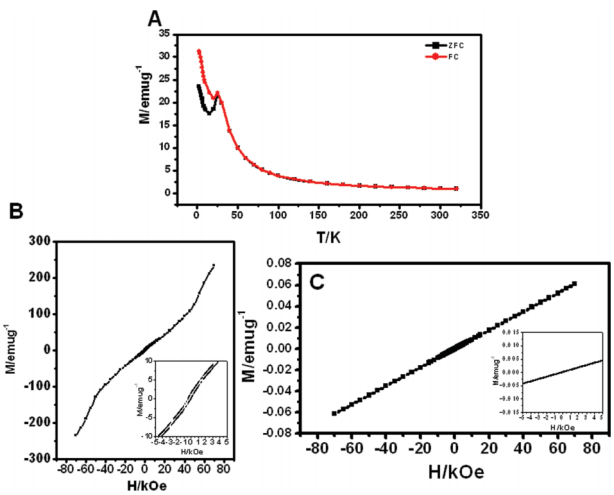

Fig. 3 Magnetic properties of hierarchical $Ni(OH)_2$ hollow spheres: (A) temperature dependence of ZFC and FC magnetization for an applied at 1 kOe and magnetic-field dependence of magnetization measured at (B) 5 K and (C) 300 K. Insets are small field range of (B) and (C), respectively.

and H_a are effective exchange field and anisotropy field, respectively.[18] Similarly, in our material, the H_e should be greatly enhanced due to the strong interaction between the $Ni(OH)_2$ plates in hollow structure, and the H_a should be also enhanced in exchange biased systems.

The thermal behavior of hierarchical $Ni(OH)_2$ hollow spheres was investigated with TG-DSC measurements in Fig. 4.

A TG curve showed that $Ni(OH)_2$ started to decompose at about 300 °C. The total weight loss was measured to be ~20% which is larger than the theoretical value (19.4%) calculated from reaction (4):

$$Ni(OH)_2 \rightarrow NiO + H_2O \quad (4)$$

The powders exhibit thermogravimetric transitions that are likely due to the loss of physically absorbed water. The weight loss in the range of 300–365 °C continued but gradually slowed at 365 °C and almost ceased at 450 °C. As a consequence, the stable residue can reasonably be ascribed to NiO. The DSC curve showed an endothermic peak with a maximum located at 345 °C. The temperature range of the endothermic peak in the DSC curve fits well with that of weight loss in the TG curve, corresponding to endothermic behavior during the decomposition of $Ni(OH)_2$ to NiO. The calcination results in the decomposition of $Ni(OH)_2$ nanosheets to NiO porous nanosheets and thus the morphology and structure of the hollow spheres were sustained very well. It was further confirmed by SEM image in Fig. 5B.

Fig. 5 shows the hierarchical NiO hollow spheres obtained from thermal decomposition of hollow spheres of $Ni(OH)_2$. The resultant hollow spheres of NiO are well crystallized, which is reflected in sharp diffraction rings of the SAED pattern and well-defined phase-pure XRD patterns of Fig. 5A and C (JCPDS card no. 04-0835). The phase transformation of $Ni(OH)_2$ to NiO causes a crystallographic structural change from the hexagonal system to the cubic system. Hollow spheres of NiO in Fig. 5B can retain the similar product morphology and size to those in Fig. 2B. EDX analysis and elemental analysis results indicated that the ratio of Ni and O is almost 1 : 1 in Fig. 5D. The TEM image of the obtained NiO hollow spheres with obvious contrast between dark edge and pale center was revealed in Fig. 5C. Fig. 5E indicated that the hollow sphere constituted of self-assembled single crystalline mesoporous nanosheets with various pore sizes. The nitrogen adsorption-desorption isotherm shows that hollow NiO have two types of hysteresis loop. It indicates the presence of meso- and macro-pores. The BET surface area of the NiO hollow spheres is 84.444 $m^2\ g^{-1}$.

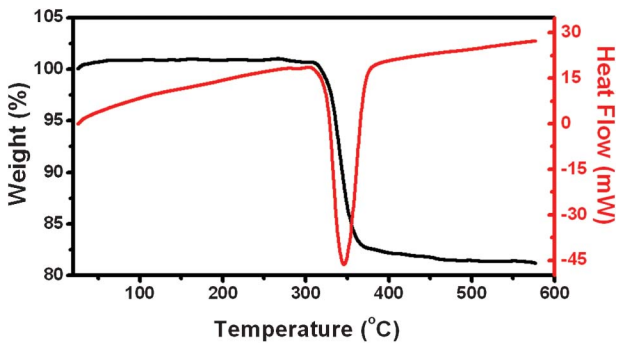

Fig. 4 Differential scanning calorimetric analysis (DSC) and thermogravimetric analysis (TG) curves of hierarchical $Ni(OH)_2$ hollow spheres.

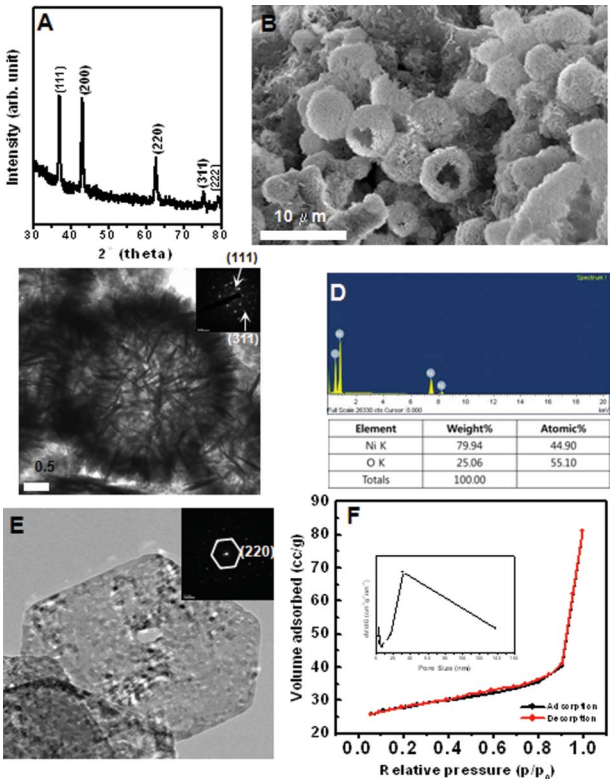

Fig. 5 (A) XRD, (B) SEM, (C) TEM, (D) EDX spectrum, (E) HRTEM image, and (F) N_2 adsorption-desorption isotherm of prepared hierarchical NiO hollow spheres. Inset are SAED patterns and pore-size distribution curve obtained from the desorption data.

The inset of Fig. 5F shows the BJH pore size distribution, showing a sharp peak at 4–6 nm, a prominent peak at 30 nm and at larger than 30 nm (broad peak).

Fig. 6A shows voltammetric behavior of the sample between 0 and 3 V at a scan rate of 0.1 mV s^{-1} in 1 M $LiPF_6$ with 50 : 50 w/w mixtures of ethylene carbonate and ethyl methyl carbonate. It is similar to the published one,[19] in which one pair of distinct redox peaks is identified. A pair of distinct redox peaks was observed, which is similar to the published one.[19] In the first cycle, the reduction occurs around 0.3 V and it corresponds to the initial reduction of NiO to metallic Ni and the formation of a partially reversible solid electrolyte interface (SEI) layer.[20] In the second cycle, the reduction potential occurring at around 1.0 V is more positive and the peak becomes broader. It is composed of a main peak at ~1.0 V and a shoulder peak around 1.3 V. The easier reduction in the second cycle implies the structural change of the material after the first scan. The presence of two reduction peaks in the second cycle indicates that there are two sets of faradaic reactions involved; (1) the reversible reaction of NiO ↔ Ni/Li_2O. (2) the partial composition/decomposition of the polymeric coating on the surface of hierarchical NiO hollow spheres. The voltammetric behavior of the third cycle is similar to second one.

Fig. 6 B and C depict the charge-discharge profiles for lithium battery performance. It is clear that as high as about 700 mAh g^{-1} of reversible capacity can be obtained at the discharge rate of 0.1 C. The rate capacity decreases, but it still remains at ~600 mAh g^{-1} at a 1 C rate. The performance of discharge capacity recovers once the charge-discharge rate changes back to 0.1 C. According to the results

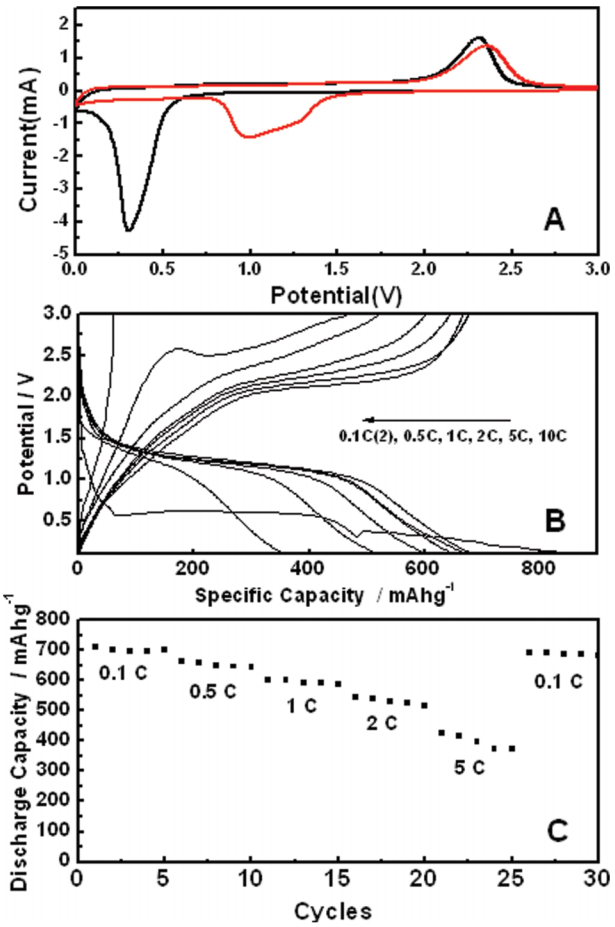

Fig. 6 (A) Cyclic voltammograms at a sweep rate of 0.1 mV s^{-1} (first scan cycle; black, second scan cycle; red) in 1 M $LiPF_6$ in 50 : 50 w/w mixtures of ethylene carbonate and ethyl methyl carbonate, (B) charge/discharge profiles, and (C) discharge capacity upon cycling at different discharge rate for the electrode made with hierarchical NiO hollow spheres.

above, the electrochemical performance of the electrode made with hierarchical hollow spheres is better than that of nanoparticles, which was reported in the other group study.[21] This is due to the high surface area of hollow spheres with mesoporous nanosheets, making a more effective electrochemical reaction with lithium. Moreover, mesoporous nanosheets are favorable for the diffusion of lithium ions, providing more active sites. In addition, the spherical structure may prohibit the agglomeration of Ni crystals to some extent, relieving the stress caused by volume changes during the charge/discharge cycles, and thereby suppressing the degradation of the hierarchical NiO hollow sphere electrode.

We have studied the magnetization behavior of NiO as function of magnetic field and temperature in Fig. 7. It is well known that bulk NiO is an antiferromagnetic material with a Neel temperature (T_N) of 525 K,[22] which is significantly higher than room temperature. The ZFC and FC curves were measured in an applied field of 1 kOe. A small discrepancy between the bifurcation temperature, T_N = 50 K and the blocking temperature T_b = 175 K is found, where T_b is defined as the peak temperature of the ZFC curve.

Zysler *et al.* proved that interparticle interactions lead to an increase in the effective anisotropy energy of the magnetic core moments, shifting the distribution of their T_b to higher temperature.[23]

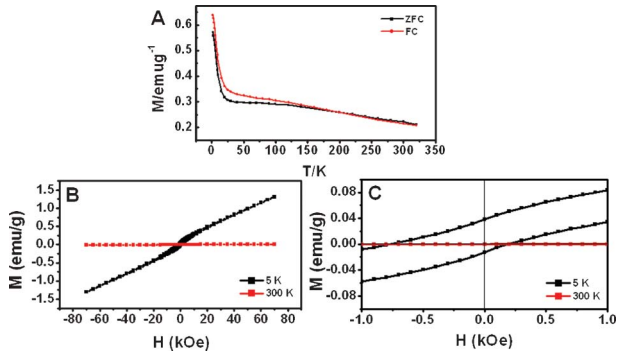

Fig. 7 Magnetic properties of hierarchical NiO hollow spheres: (A) temperature dependence of ZFC and FC magnetization for an applied field at 1 kOe and (B) magnetic hysteresis loop at 5 K and 300 K. (C) A small field range of (B).

The interparticle interactions are stronger and will be able to shift T_b and T_N compared with the NiO nanoparticles. Fig. 7 B and C show the magnetization curves at 5 and 300 K. At 5 K, an asymmetric hysteresis loop was observed in Fig. 7 C. This loop shift to the left is most likely linked to the exchange bias between the surface layer and the inner core in coupled system; *i.e.* the uncompensated spin of the surface Ni sites and Ni atoms surrounding the holes in the present study largely contribute to the net magnetic moment of the sample due to the breaking of the crystal symmetry. At 300 K in Fig. 7 B, all spins turn to antiferromagnetic coupling when the temperature is over T_N (T_N = 95 K). An increase of the thermal energy would trade off to diminish the spin ordering and exchange bias, resulting in the disappearance of the hysteresis. Hierarchical NiO hollow spheres with single crystalline nanosheets from hierarchical $Ni(OH)_2$ hollow spheres were prepared by hydrothermal treatment and calcination in air. Even though the shapes of the hollow $Ni(OH)_2$ spheres were completely retained during the calcination, the surface area of these was increased due to the creation of mesopores in the nanosheets by dehydration of $Ni(OH)_2$ during calcination in air.

The magnetic hysteresis measurements show interesting behaviors such as Neel temperature and blocking temperature. Also the test of the electrochemical performance for lithium ion shows better results compared with other reports because hierarchical NiO hollow spheres have single crystalline mesoporous nanosheets. Owing to the facile method in preparing hierarchical NiO hollow sphere and its superior capacity, they can be applied in other fields such as sensors, magnetic sensors, catalytic fields, hydrogen storage, *etc.*

Acknowledgements

This work was supported by the Korea Center for Artificial Photosynthesis (KCAP) located in Sogang University funded by the Ministry of Education, Science, and Technology (MEST) through the National Research Foundation of Korea (NRF-2011-C1AAA001-2011-0030278).

References

1 T. Rueckes, K. Kim, E. Joselevich, G. Y. Tseng, C. L. Cheung and C. M. Lieber, *Science*, 2000, **289**, 94.
2 Y. Li, B. C. Zhang, X. W. Xie, J. L. Liu, Y. D. Xu and W. J. Shen, *J. Catal.*, 2006, **238**, 412.

3 P. Poizot, S. Laruelle, S. Grugeon, L. Dupont and J.-M. Tarascon, *Nature*, 2000, **407**, 496.
4 P. Poizot, S. Laruelle, S. Grugeon and J.-M. Tarascon, *J. Electrochem. Soc.*, 2002, **149**, A1212.
5 B. Sheela, H. Gomathi and G. P. Rao, *J. Electroanal. Chem.*, 1995, **394**, 267.
6 M. Chigane and M. Ishikawa, *J. Chem. Soc., Faraday Trans.*, 1992, **88**, 2203.
7 C. R. Makkus, K. Hemmes and D. W. Wir, *J. Electrochem. Soc.*, 1994, **141**, 3429.
8 H. Kumagai, M. Matsumoto, K. Toyoda and M. Obara, *J. Mater. Sci. Lett.*, 1996, **15**, 1081.
9 (*a*) F. F. Ferreira, M. H. Tabacnikes, M. C. A. Fantini, I. C. Faria and A. Gorenstein, *Solid State Ionics*, 1996, **971**, 86.
10 K.-F. Chiu, C. Y. Chang and C. M. Lin, *J. Electrochem. Soc.*, 2005, **152**, A1188.
11 R. H. Kodama, S. A. Makhlouf and A. E. Berkowitz, *Phys. Rev. Lett.*, 1997, **79**, 1393.
12 D. Wang, C. Song, Z. Hu and X. Fu, *J. Phys. Chem. B*, 2005, **109**, 1125.
13 H. Cölfen and S. Mann, *Angew. Chem., Int. Ed.*, 2003, **42**, 2350.
14 D. Walsh and S. Mann, *Nature*, 1995, **377**, 320.
15 H. Cölfen and M. Antonietti, *Angew. Chem., Int. Ed.*, 2005, **44**, 5576.
16 Y. Wang, Q. Zhu, L. Tao and X. Su, *J. Mater. Chem.*, 2011, **21**, 9248.
17 T. Takada, Y. Bando, M. Kiyama and H. Miyamoto, *J. Phys. Soc. Jpn.*, 1996, **21**, 2745.
18 D. L. Mills, *Phys. Rev. Lett.*, 1968, **20**, 18.
19 S. A. Needham, G. X. Wang and H. K. Liu, *J. Power Sources*, 2006, **159**, 254.
20 M. H. Park, M. G. Kim, J. Joo, K. Kim, J. Kim, S. Ahn, Y. Cui and J. Cho, *Nano Lett.*, 2009, **9**, 3844.
21 Z. Yuqin and W. Yong, *Rare Met.*, 2011, **30**, 59.
22 J. S. Smart and S. Greenwald, *Phys. Rev.*, 1951, **82**, 1134.
23 E. Winkler, R. D. Zysler, M. V. Mansilla, D. Fiorani, D. Rinaldi, M. Vasilakaki and K. N. Trohidou, *Nanotechnology*, 2008, **19**, 185702.